Systems & Control Transactions

Research Article
Foundations of Computer Aided Process Design (FOCAPD 2024)
Breckenridge, Colorado, USA. July 14-18, 2024
Peer Reviewed Conference Proceeding

PSE PRESS

Simulation and Comparative Analysis of Conventional Steam-Methane Reforming Models for Reactor Electrification

Yufei Zhao[a], Chengtian Cui[a], and Cornelius. M. Masuku[a]*

[a] Purdue University, Davidson School of Chemical Engineering, West Lafayette, Indiana, USA
* Corresponding Author: cmasuku@purdue.edu.

ABSTRACT

This study delves into the development and examination of various mathematical models for conventional steam-methane reforming (SMR) reactors, establishing a foundational basis for an electrified SMR reactor design. Distinct mathematical models with different scales and dimensions are derived. A basic 1D-fluid, 0D-catalyst (1D-0D) pseudo-homogeneous model is validated with plant data, and progressively advanced to a 2D-0D model considering radial transfer, then further extended to a rigorous 2D-1D model considering transfer phenomena between catalyst particle and fluid. Simulation cases are conducted under uniform design parameters, heat source and operation conditions. Comparative analyses focus on several key performance aspects, including temperature, reaction rate distribution, and outlet characteristics such as temperature, pressure, flow rate, composition and CH_4 conversion. The models effectively describe the industrial SMR reactor behavior. Influences of scale and dimension of mathematical model on reactor performance are highlighted. The rigorous 2D-1D model is identified as the most suitable model for adapting to electrified reactor configurations due to its precise capture of transfer phenomena and detailed illustration of both fluid and catalyst behaviors.

Keywords: Steam Methane Reforming, Reactor Design, Multi-Scale Modeling, Decarbonization, Hydrogen Production.

1 INTRODUCTION

Hydrogen (H_2) is a crucial industrial chemical with a reported demand of approximately 90 million tonnes in the year 2020 and a projected increase in demand ranging from 28% to 45% by 2030 [1]. H_2 plays a vital role in various sectors including oil refining, and ammonia production among others [2]. About 62% of H_2 is produced from natural gas especially through steam-methane reforming (SMR) [1]. However, conventional SMR has disadvantages including: consumption of fossil fuels, emissions of carbon dioxide, heat transfer limitation of tube-furnace design. Electrification through induction heating as a substitute of heat source presents a noteworthy alternative [3]. To numerically assess an electrically-heated SMR (E-SMR), an electromagnetic model for induction heating is required. Concurrently, a comprehensive SMR model that can correlate the heat generation at catalyst sites with the overall behavior of the reactor is essential.

There has been abundant research about modeling of SMR reactor. Latham *et al.* [4] developed a mathematical model of the reformer by segments which were discretized axially. Constant effectiveness factors were implemented with intrinsic kinetic model for reaction rate calculation. The model can predict temperature profiles for the outer-tube wall, inner-tube wall, furnace gas and process gas. Kuncharam, B. V. R *et al.* [5] employed a multi-scale modeling approach, integrating a steady state two-dimensional model for fluid-phase with a one-dimensional model for the pellet-phase. The effectiveness factor assumption was avoided. Their findings assert that the application of the Ergun equation to calculate the pressure drop in SMR reformer yields satisfactory results. Furthermore, the incorporation of molar change is necessary. Tacchino *et al.* [6] presented a validated

steady state multi-scale model of an industrial SMR reactor comprised of the furnace and reformer. A significant variability in effectiveness factor was observed, indicating the necessity of including catalyst particle simulation. The model proved its robustness by showing no sensitive reliance on adjustable parameter, the flame length.

Current advances in SMR modeling reveal a notable discrepancy in the approaches across different scales and dimensions. Models have been developed based on distinct parameters, operating conditions, and empirical expressions. Key factors such as fluid mechanics, heat input, temperature and reaction rate distributions, showing significant influence on the overall behavior including outlet condition, CH_4 conversion and efficiency of the reformer, have dependencies on scale and dimensionality. There lacks a comprehensive comparative analysis rooted in a uniform basis. In order to lay a foundation for E-SMR model development, and to quantify the key factors and the influence of varied-scale and varied-dimension on reactor behavior, numerical simulation of different models and analysis are required [7].

In this paper, for fluid-catalyst dimensions, 1D-0D, 2D-0D, 2D-1D mathematical models of conventional SMR are developed based on the same design parameters and operation conditions. Temperature and reaction rate distributions corresponding to different scenarios are illustrated. SMR reactor properties are recognized. Outlet behaviors, including temperature, pressure, flow rate, composition and CH_4 conversion are observed. Sensitivity analysis is conducted for the radial conductivity. Differences of the modeling schemes are recognized and analyzed.

2 MODEL DEVELOPMENT

Table 1: Characteristics of reactor tube and catalyst particles.

Parameters	Value	Unit
Length of tube	12.5	m
Radius of tube	0.063	m
Diameter of catalyst	0.0035	m
Conductivity of catalyst	33	W/m/K
Density of catalyst	3690	kg/m^3
Heat capacity of catalyst	880	J/kg/K

Industrial SMR reactors contain parallel tubes arranged in rows and columns inside the furnace, each packed with catalyst. This paper sets up a mathematical model of an industrial-scale single tube to observe the overall behavior of the reactor. Ni/$MgAl_2O_4$ catalyzes the reaction. Characteristics of reactor tube and catalyst particles are listed in Table.1.

The following assumptions have been made for establishing the models:

2.1 Assumptions

1. Operational conditions and performance data can be linearly extrapolated from a single tube to the overall reactor;
2. The fluid phase follows ideal gas behaviors;
3. Spherical catalyst particle and cylindrical tube have constant porosity respectively;
4. 3 main reactions occur:

$$CH_4 + H_2O \leftrightarrow CO + 3H_2 \quad \Delta H_1^{298K} = 206.1 kJ/mol \quad (1)$$

$$CO + H_2O \leftrightarrow CO_2 + H_2 \quad \Delta H_2^{298K} = -41.15 kJ/mol \quad (2)$$

$$CH_4 + 2H_2O \leftrightarrow CO_2 + 4H_2 \quad \Delta H_3^{298K} = 164.95 kJ/mol \quad (3)$$

5. Inner tube wall temperature is a polynomial function of axial space position fitted from industrial data.

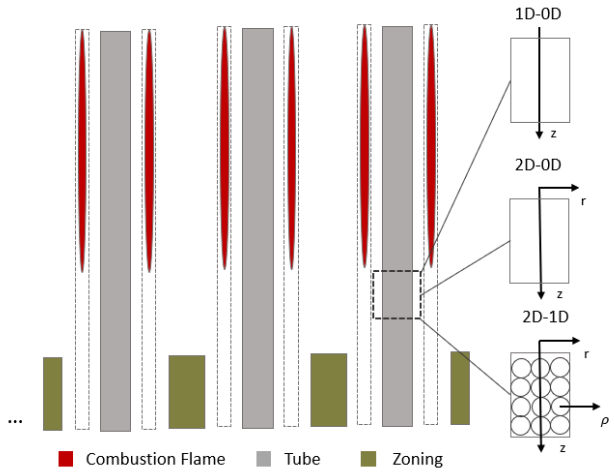

Figure 1. Abbreviated diagram of industrial SMR reactor (reproduced from Ref. [4]) and illustration of three models regarding scale and dimension.

Three models covering different scales and dimensions are shown in Figure 1, along with industrial SMR reactor diagram. Tube expressions are derived in cylindrical coordinate, while catalyst particle expressions in spherical coordinate. Considering geometric symmetry, the most rigorous scenario is a multi-scale model considering multi-dimension including axial and radial domains for the fluid phase in tube, and radial domain for catalyst particle (2D-1D). Additional assumptions may be included owing to the distinct characteristics in each model. In the 2D-0D model, reactor tube is assumed to be pseudo-homogeneous simplifying the heterogeneity. For 1D-0D model, plug flow behavior is additionally assumed.

Table 2: Nomenclature.

Symbol	Unit	Name
C	mol/m^3	concentration
u	m/s	Interstitial velocity
U	m/s	Superficial velocity
D	m^2/s	diffusivity
y		Composition
f	Hz	Frequency of alternating magnetic field
a_p	m^2/m^3	surface area per unit volume of catalyst
d_p	m	diameter of catalyst
R_{tube}	m	Radius of reactor tube
k_m	m/s	solid-fluid mass transfer coefficient
k_h	W/m$^{2/}$K	solid-fluid heat transfer coefficient
ρ_f	kg/m^3	density of fluid
ρ_p	kg/m^3	density of catalyst particle
c_p	J/kg/K	heat capacity
T	K	temperature
λ	W/m/K	conductivity
R	mol/kgcat/s	reaction rate
L	m	length of reactor tube
ΔH	J/mol	reaction enthalpy
ε		porosity
ν		stoichiometry of reactions
h	W/m^2/K	Tube-fluid heat transfer coefficient
A_{hys}	J/kg	Hysteresis area
Pr	$\mu c_p/\lambda$	Prandtl number
Pe	ud/D_i	Peclet number
Re	$\rho ud/\mu$	Reynolds number
Sh	$k_m d/D_i$	Sherwood number
Sc	$\mu/Di/\rho$	Schmidt number
Subscript		
i,j		component or reaction index
z		fluid axial domain
r		fluid radial domain
ρ		catalyst radial domain
s		catalyst surface
b		catalyst bed
f		Fluid phase
p		Catalyst phase
Superscript		
e		effective coefficient
eo		quiescent bed effective coefficient

2.2 Mathematical Expressions

The mathematical models encompass mass, heat and momentum conservations under steady state for fluid mechanics description, and kinetic model for reaction description. Mass diffusion and convection, and heat conduction and convection, are considered for transfers. Pressure drop expression is derived from momentum conservation with friction factor calculated by the Ergun equation.

For the purpose of elucidating the expressions, the rigorous 2D-1D model is shown below as a representative example since it is the most detailed.

2.2.3 Fluid Phase

2.2.3.1 Mass Conservation

$$\frac{\partial C_i}{\partial z}u_z + C_i\frac{\partial u_z}{\partial z} = \frac{1}{r}D^e_{i,r}\frac{\partial C_i}{\partial \mathrm{r}} + \frac{\partial D^e_{i,r}}{\partial \mathrm{r}}\frac{\partial C_i}{\partial \mathrm{r}} + D^e_{i,r}\frac{\partial^2 C_i}{\partial r^2} + \frac{\partial D^e_{i,z}}{\partial z}\frac{\partial C_i}{\partial z} + D^e_{i,z}\frac{\partial^2 C_i}{\partial z^2} + \frac{(1-\varepsilon_b)}{\varepsilon_b}a_p k_{i,m}(C_{i,s} - C_i) \quad (1)$$

Boundary conditions:

$$C_i|_{z=0} = c_{i0};\ \frac{\partial C_i}{\partial \mathrm{z}}|_{z=L} = 0;$$

$$\frac{\partial C_i}{\partial \mathrm{r}}|_{r=0} = 0;\ \frac{\partial C_i}{\partial \mathrm{r}}|_{r=R_{tube}} = 0 \quad (2)$$

2.2.3.2 Heat Conservation

$$\varepsilon_b\rho_f u_z c_p\frac{\partial \mathrm{T}}{\partial \mathrm{z}} = \frac{1}{\mathrm{r}}\lambda^e_r\frac{\partial \mathrm{T}}{\partial \mathrm{r}} + \frac{\partial \lambda^e_r}{\partial \mathrm{r}}\frac{\partial \mathrm{T}}{\partial \mathrm{r}} + \lambda^e_r\frac{\partial^2 \mathrm{T}}{\partial r^2} + \frac{\partial \lambda^e_z}{\partial z}\frac{\partial \mathrm{T}}{\partial \mathrm{z}} + \lambda^e_z\frac{\partial^2 \mathrm{T}}{\partial z^2} + (1-\varepsilon_b)a_p k_h(\mathrm{T_s} - \mathrm{T}) \quad (3)$$

Boundary conditions:

$$-\lambda^e_r\frac{\partial \mathrm{T}}{\partial \mathrm{r}}|_{r=R_{tube}} = \mathrm{h}(T_w - T);\ \frac{\partial \mathrm{T}}{\partial \mathrm{r}}|_{r=0} = 0;$$

$$T|_{z=0} = T_0;\ \frac{\partial T}{\partial z}|_{z=L} = 0 \quad (4)$$

2.2.4 Catalyst Phase

2.2.4.1 Mass Conservation

$$0 = \frac{2}{\rho}D_{i,p,\rho}\frac{\partial C_{i,p}}{\partial \rho} + \frac{\partial D_{i,p,\rho}}{\partial \rho}\frac{\partial C_{i,p}}{\partial \rho} + D_{i,p,\rho}\frac{\partial^2 C_{i,p}}{\partial \rho^2} + \frac{1}{\varepsilon_p}\rho_p\sum_{j=1}^{3}\nu_{ij}R_j \quad (5)$$

Boundary conditions:

$$\frac{\partial\, \mathrm{C_{i,p}}}{\partial \rho}|_{\rho=0} = 0;\ -\varepsilon_p D_{i,p_\rho}\frac{\partial C_{i,p}}{\partial \rho}|_{\rho=R_p} = k_{i,m}(C_{i,s} - C_i) \quad (6)$$

2.2.4.2 Heat Conservation

$$\left[(1-\varepsilon_p)\rho_p c_{p,p} + \varepsilon_p\rho_f c_{p,f}\right]\frac{\partial T_p}{\partial t} = \frac{2}{\rho}\lambda^e_{p,\rho}\frac{\partial T_p}{\partial \rho} + \frac{\partial \lambda^e_{p,\rho}}{\partial \rho}\frac{\partial T_p}{\partial \rho} + \lambda^e_{p,\rho}\frac{\partial^2 T_p}{\partial \rho^2} - (1-\varepsilon_p)\rho_p\sum_{j=1}^{3}R_j\,\Delta H_j \quad (7)$$

Boundary conditions:

$$\frac{\partial T_p}{\partial \rho}|_{\rho=0} = 0;\ -\lambda^e_{p,\rho}\frac{\partial T_p}{\partial \rho}|_{\rho=R_p} = k_h(T_s - T) \quad (8)$$

2.2.5 Coefficients

2.2.5.1 Diffusivity

Axial and radial effective diffusivity are expressed as following:

$$\frac{1}{Pe_z} = \frac{0.72}{Re_p Sc} + \frac{0.52}{\left(1+\frac{9.0}{Re_p Sc}\right)} \quad (9)$$

$$\frac{1}{Pe_r} = \frac{0.34}{(Re_o Sc)^{0.80}} + \frac{0.08}{\left(1+\frac{10.8}{Re_o Sc}\right)} \quad (10)$$

2.2.5.2 Conductivity

$$\frac{\Lambda_r^e}{\lambda_f} = \frac{\lambda^{eo}}{\lambda_f} + 0.1\mathrm{PrRe} \quad (11)$$

$$\frac{\lambda_z^e}{\lambda_f} = \frac{\lambda^{eo}}{\lambda_f} + 0.5PrRe \quad (12)$$

2.2.5.3 Solid-fluid transfer coefficient

$$Sh = \frac{k_{i,m} d_p}{D_{i,m}} = 2 + 1.1Sc^{1/3}Re_o^{0.6} \quad (13)$$

$$Nu = \frac{k_h d_p}{\lambda_m} = 2 + 1.1Pr^{1/3}Re_o^{0.6} \quad (14)$$

2.2.5.4 Tube-fluid heat transfer coefficient

$$\mathrm{H} = \alpha \frac{\lambda}{d_p}\left(2.58\mathrm{Re}^{\frac{1}{3}}\mathrm{Pr}^{\frac{1}{3}} + 0.094\mathrm{Re}^{0.8}\mathrm{Pr}^{0.4}\right) \quad (15)$$

2.2.6 Kinetics

An intrinsic Langmuir-Hinshelwood-Hougen-Watson kinetic model developed by Xu and Froment [8] is applied.

3 RESULTS

The equation-based mathematical models composed of PDEs are coded in FORTRAN and solved in Aspen Custom Modeler V12.1. Physical properties are calculated by calling Aspen properties bank. Finite difference methods are used for discretization. Newton Method solves the system of nonlinear equations.

3.1 1D-0D Model Validation

This model describes homogeneous reactor tube with only axial domain transfer. The simulation has 9,887 equations after decomposition. Operating conditions of the three cases implemented are listed in Table 3.

The model validation focuses on temperature profile along the tube, CH_4 conversion of methane and outlet pressure. Root mean standard error (RMSE) and Pearson correlation Coefficient (PCC) defined in Equation 16 are calculated to measure deviation and correspondence of change tendency of profile. The smaller RMSE is, and the closer CF is to 1, the better consistency the simulated profile shows to industrial case. Relative error (RE) is calculated for evaluating CH_4 conversion and pressure. Figure 2 shows comparative results between temperature profile derived from our model and those documented in literature under Case 3 operation conditions as an example. Modeled composition profiles are plotted in Figure 3, along with industrial outlet values. Table 4 shows the evaluation coefficients quantifying the comparison of temperature profile. The developed 1D-0D model has lowest PCC of 0.9979, highest RE of 3.61%, highest RMSE of 14.28 compared with 800-1150K range, showing a consistency with literature reported. The outlet behaviors are listed in Table 5. The results are aligned with plant data.

$$CF = \frac{\sum(x-\bar{x})(y-\bar{y})}{\sqrt{\sum(x-\bar{x})^2(y-\bar{y})^2}} \quad (16)$$

Heat is input into a discretized plug flow segment for 1D-0D model. The profile is plotted in Figure 4 along with reaction rate. The maximum heat input is reached at about L=3-5m, which is the length of a combustion flame. The majority of reactions happen near the entrance of the tube length area, leading to a temperature drop to minimum at about L=0.625m.

Table 3: Inlet operation conditions of 3 industrial cases [4].

	Case1	Case2	Case3
T [K]	884.55	887.05	879.85
P [bar]	30.060	29.440	28.085
Velocity [m/s]	1.279	1.147	0.925
y_{CH4}	0.2421	0.2487	0.2401
y_{H2O}	0.7461	0.7377	0.7437
y_{CO}	0.0036	0.0042	0.0060
y_{CO2}	0.0047	0.0053	0.0042
y_{H2}	0.0036	0.0042	0.0060

Table 4: Evaluation coefficients of 3 cases compared with literature documented [4].

	Case1	Case2	Case3
RMSE	14.28	12.58	10.46
PCC	0.9979	0.9981	0.9979

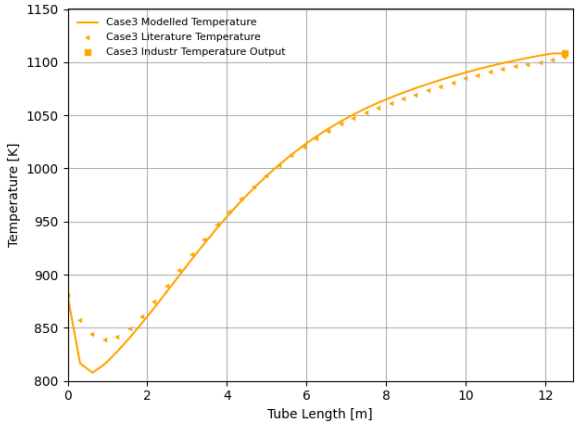

Figure 2. Simulated (solid), literature (dashed) temperature profile along the tube of Case 3 with RMSE of 10.4.

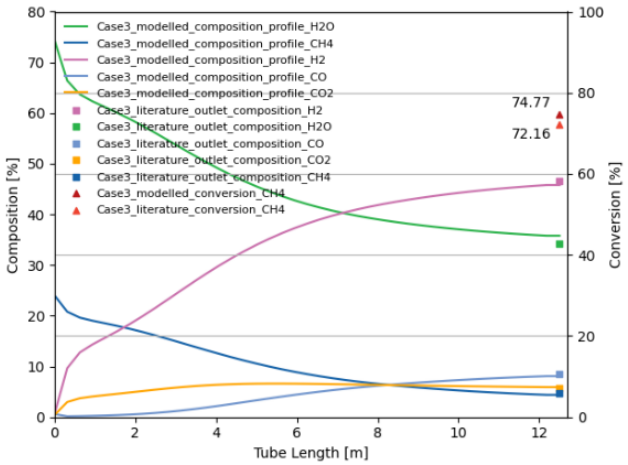

Figure 3. Simulated industrial composition profile along the tube, and CH_4 conversion of case 3.

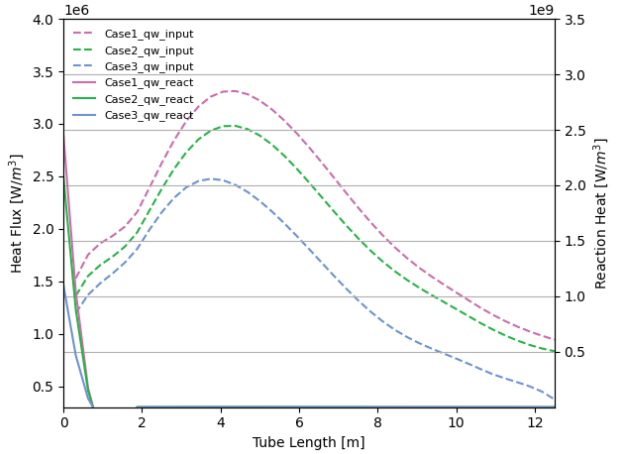

Figure 4. Simulated reaction heat (solid) and input heat (dashed) profile along the tube.

3.2 2D-0D Model

Radial transfer is introduced in 2D-0D homogenous model based on 1D-0D model. The simulation has 43,035 equations after decomposition. Case 3 is implemented for comparison.

Figure 5 shows simulated temperature distribution. Axially lowest temperature appeared at L=0.3125-0.625m, which is at similar position compared with 1D-0D. Radial temperature difference is observed, with a highest of 126.31K at L=4.0625m, which is slightly delayed compared with the maximum heat input at L=3.75m. Radial temperature difference follows the same trend as heat input as shown in Figure 6 (top). Radial temperature difference indicating heat loss is inevitable considering the relatively low radial heat transfer efficiency. However, the average temperature along axial direction still shares a similar trend compared with 1D-0D. 2D-0D case has a lower average temperature of 49.4K, leading to a CH_4 conversion decrease from 75% to 64%.

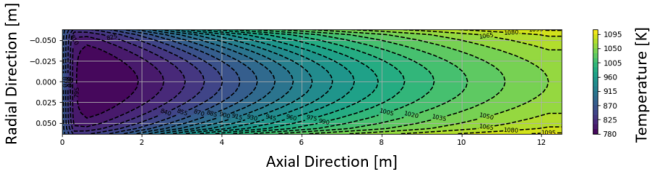

Figure 5. Simulated temperature distribution in 2D-0D case.

Figure 7 illustrates the distribution of the reaction rate, using Reaction 3 as a representative case. 99.5% of the overall reaction occurs with the length L=0.9375m. For the rest of the tube length, 69%-83% of the reaction occurs near the reactor tube wall where temperature is highest radially, indicating the reactor being heat transfer limited.

The different behaviors between 2D-0D and 1D-0D are resulted from with or without plug-flow assumption. Radial transfer coefficient is assumed to be infinitely large to reach uniform distribution. This tendency is illustrated in Figure 8 that the larger the radial conductivity is, the closer the average outlet temperature is to 1D-0D model.

Table 5: Modelled outlet behaviors compared with industrial data [4].

	Case 1	Plant 1	Case 2	Plant 2	Case 3	Plant 3
Temperature [K]	1107.51	1105.55	1108.77	1107.15	1108.25	1108.95
Pressure [bar]	28.461	28.189	28.040	27.990	27.234	27.155
Flow Rate [mol/s]	8.935	8.970	7.797	8.082	6.136	6.024
CH_4 Conversion [%]	73.79	71.30	73.11	70.70	74.77	72.16
y_{CH4}	0.0461	0.0505	0.0484	0.0526	0.0482	0.0440
y_{H2O}	0.3614	0.3507	0.3517	0.3417	0.3430	0.3580
y_{H2}	0.4544	0.4583	0.4593	0.4631	0.4655	0.4580
y_{CO}	0.0790	0.0820	0.0820	0.0845	0.0850	0.0808
y_{CO2}	0.0591	0.0582	0.0587	0.0575	0.0574	0.0592

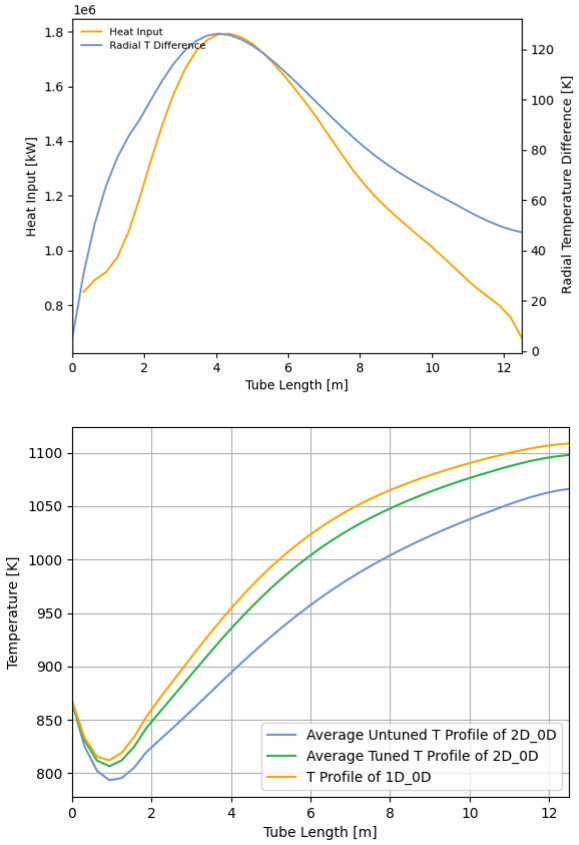

Figure 6. (top) Heat input profile (left) and radial temperatue difference (right) profile along the reactor tube; (bottom) 1D-0D temperature profile, untuned and tuned 2D-0D average temperature profile.

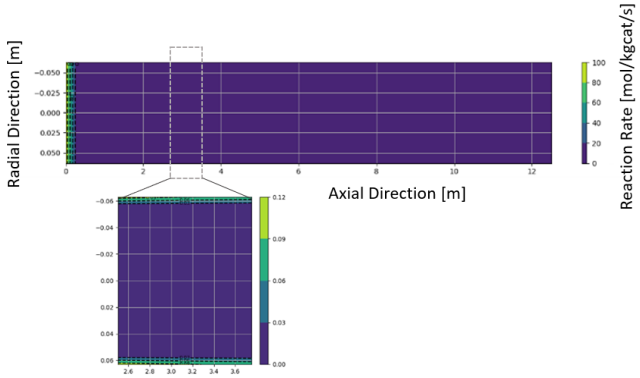

Figure 7. Reaction rate distribution in reactor tube with as a function of a specific length.

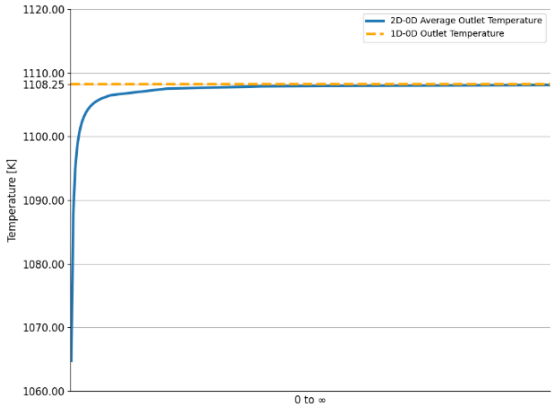

Figure 8. 2D-0D average outlet temeprature versus radial conductivity.

To ensure that the 2D model has better accordance with industrial data regarding the CH_4 conversion, the amount of heat input is recalculated by parameter tuning of the tube-fluid heat transfer coefficient α. The tuned-conversion reaches less than 5e-4% RE compared with industrial data. Heat input after tuning has an average of 1.7e5 W/m^3 more in amount compared with untuned case. Outlet average temperature has 1.03% RE, while pressure has 0.15% RE. The tuned temperature distribution has an average temperature of 14.3K lower than 1D-0D due to the radial temperature distribution, but 35.1K higher than untuned 2D-0D shown in Figure 6 (bottom). The outlet behaviors are listed in Table 6. The tuned case approaches the plant data more than untuned case.

Table 6. Comparison of tuned, untuned 2D-0D cases and industrial case.

Outlet	Tuned	Untuned	Plant
Temperature [K]	1096.86	1064.77	1108.95
Pressure [bar]	27.19	27.25	27.23
Flow Rate [mol/s]	6.133	6.015	6.024
CH_4 Conversion [%]	72.16	64.32	72.16
y_{CH4}	0.0496	0.0560	0.0482
y_{H2O}	0.3661	0.3756	0.3430
y_{H2}	0.4480	0.4364	0.4655
y_{CO2}	0.0605	0.0619	0.0573
y_{CO}	0.0757	0.0702	0.0850

3.3 2D-1D Model

Solid catalyst particle phase is taken into consideration for 2D-1D heterogenous model. External transfer between catalyst surface and fluid phase, and internal transfer in catalyst particle are introduced. The simulation has 205,389 equations after decomposition. Case 3 is implemented for comparison.

Temperature difference exists between the fluid, the catalyst surface, and catalyst center, leading to

additional heat loss. Figure 9 (a) shows the temperature distribution of fluid. Temperature differences from catalyst center to catalyst surface is less than 0.5 K. Temperature difference from catalyst surface to fluid distribution is shown in Figure 9 (b), the average is 3.69 K. The maximum difference axially is at entrance, while radially is at tube wall, where the majority of reactions occur, which is consistent with 2D-0D observation. A drop in CH_4 conversion of 24% is observed under the same condition as 2D-0D.

Reaction rate distributions of catalyst particle at specific positions are shown in Figure 10. The majority of reactions occur near the surface, which indicates that the catalytic reactions are diffusion-limited.

The outlet behaviors are shown in Table 7. The 2D-1D outlet behaviors show good consistency with 2D-0D case, except temperature and CH_4 conversion.

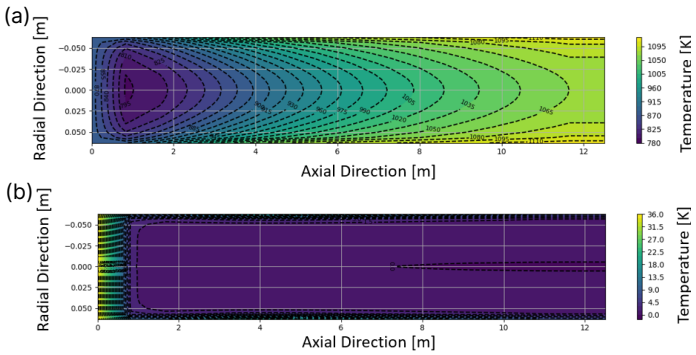

Figure 9. (a) Temperature dfistribution of 2D-1D fluid phase; (b) Temperature difference between fluid and catalyst surface distribution of 2D-1D.

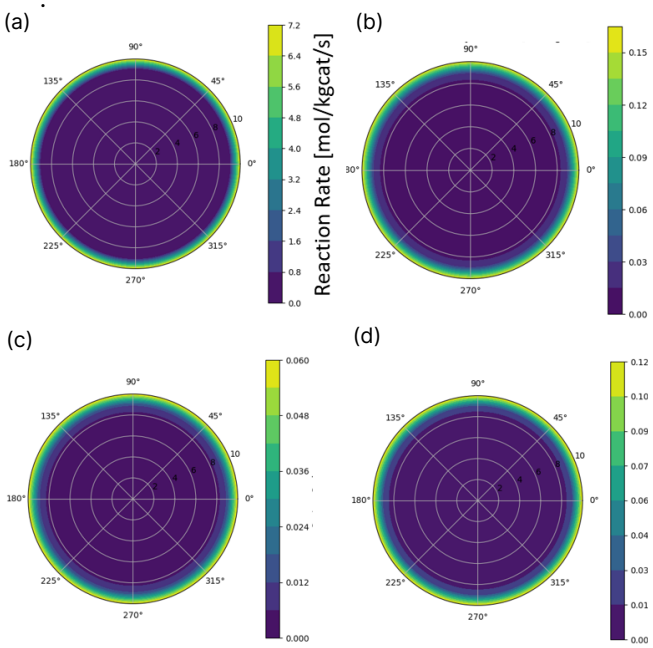

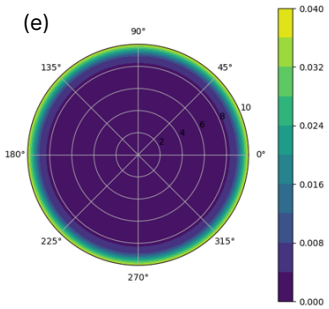

Figure 10. Reaction rate distitbution of catalyst particle at position (a) L/L_{tube}=0; (b) L/L_{tube}=0.20; (c) L/L_{tube}=0.47; (d) L/L_{tube}=0.73; (e) L/L_{tube}=1.

Table 7. Comparison of 2D-1D with tuned 2D-0D cases.

Outlet	2D-1D	2D-0D
Temperature [K]	1080.09	1096.86
Pressure [bar]	27.19	27.19
Flow Rate [mol/s]	6.083	6.133
CH_4 Conversion [%]	47.99	72.16
y_{CH4}	0.0498	0.0496
y_{H2O}	0.3665	0.3661
y_{H2}	0.4481	0.4480
y_{CO2}	0.0606	0.0605
y_{CO}	0.0750	0.0757

3.4 E-SMR Model

The development of conventional SMR model lays foundation for heat electrification that E-SMR model is developed by incorporation of induction heat model. Hysteresis heat is regarded as dominant induction heat source, which is estimated by the following expression:

$$P_{hys} = A_{hys} f \rho \qquad (17)$$

where hysteresis area A_{hys} is dependent on material electromagnetic property, magnetic field strength and temperature.

In conventional SMR reactors, the heat flux source is introduced as a boundary condition for the fluid phase boundary at tube layer. While for induction-heated E-SMR reactor which utilizes dual-function catalysts, heat is directly generated at the catalyst sites. The heat flux is introduced internally from the catalyst phase in the way that the P_{hys} term is included as a source term in the energy conservation equation of the catalyst/fluid phase.

4 CONCLUSIONS

Mathematical models covering varied scales and dimensions of SMR Reactor tube have been developed. Comparative analyses have been carried out focusing on

temperature, reaction rate distribution and outlet behaviors, including temperature, pressure, flow rate, composition and CH_4 conversion.

Validation with industrial data shows that the 1D-0D numerical simulation can precisely describe the SMR reactor behavior. When developed on the same basis, the 2D-0D shows a radial temperature distribution. When resistance of radial transfer is set to infinitely small, the behavior of 2D-0D is approaching 1D-0D, which is a validation of the developed 2D-0D model. Higher reaction rates are mainly distributed near entrance and near tube wall positions, indicating a heat transfer limited property. 2D-0D shows a lower CH_4 conversion than 1D-0D considering the heat resistance behavior in the way of radial temperature distribution. A heat transfer coefficient corresponding to industrial plant CH_4 conversion can be obtained by parameter fitting. The fitted 2D-0D case shows a high correlation with plant data. 2D-1D model was further developed with the results showing additional heat resistance in the way of temperature difference between the fluid, catalyst surface, and catalyst center. A further decrease of CH_4 conversion compared with 2D-0D is observed. On catalyst sites, the majority of reactions occur at position close to the catalyst surface, indicating the diffusion-limited property.

Simplification of model in terms of scale and dimension neglects some of the heat resistances. Due to the fixed tube wall assumption for all three cases, and same initial conditions, the neglected heat resistance manifests in the way of decreased CH_4 conversion. However, distinct models are suitable for different tasks. When an estimation of effectiveness factor is unavailable and catalyst behaviors are required, rigorous 2D-1D is more suitable.

ACKNOWLEDGEMENTS

The authors would like to thank the Center for Innovative and Strategic Transformation of Alkane Resources (CISTAR) and the National Science Foundation under Cooperative Agreement No. EEC-1647722 for funding.

REFERENCES

1. International Energy Agency. Global Hydrogen Review 2022. (2022)
2. Department of Energy. https://www.energy.gov/eere/fuelcells/h2scale
3. Wismann ST, et al. Electrified methane reforming: A compact approach to greener industrial hydrogen production. Science 364(6442): 756-759 (2019).
4. Latham DA. Mathematical Modelling of an Industrial Steam-Methane Reformer. PhD Thesis, Queen's University, Kingston, ON (2008).
5. Kuncharam BVR, Dixon AG. Multi-scale two-dimensional packed bed reactor model for industrial steam methane reforming. Fuel Process Technol 200 :106314 (2020).
6. Tacchino V, et al. Multi-scale model of a top-fired steam methane reforming reactor and validation with industrial experimental data. Chem Eng J 428: 131492 (2022).
7. Masuku CM, et al. Process decarbonization through electrification. Curr Opin Chem Eng 44: 101011 (2024).
8. Xu J, Froment GF. Methane steam reforming: II. diffusional limitations and reactor simulation. AIChE J 35: 97–103 (1989).